JPET Fast Forward. Published on October 30, 2017 as DOI: 10.1124/jpet.117.243931
This article has not been copyedited and formatted. The final version may differ from this version.

JPET #243931

Title Page

Title

Pharmacokinetic/Pharmacodynamic Modeling of Schedule-Dependent Interaction between Docetaxel and Cabozantinib in Human Prostate Cancer Xenograft Models

Author names and affiliations

Wenjun Chen, Rong Chen, Jian Li, Yu Fu, Liang Yang, Hong Su, Ye Yao, Liang Li, Tianyan Zhou, Wei Lu

Beijing Key Laboratory of Molecular Pharmaceutics and New Drug Delivery System, Department of Pharmaceutics, School of Pharmaceutical Sciences, Peking University, Beijing 100191, China.

Running Tittle Page

Running title: PK/PD modeling of schedule-dependent drug combination in mice

Corresponding author:

Tianyan Zhou

Beijing Key Laboratory of Molecular Pharmaceutics and New Drug Delivery System, Department of Pharmaceutics, School of Pharmaceutical Sciences, Peking University, Beijing 100191, China.

Tel.: +8610-82805937 Fax: +8610-82805937

E-mail address: tianyanzhou@bjmu.edu.cn

Wei Lu

Beijing Key Laboratory of Molecular Pharmaceutics and New Drug Delivery System, Department of Pharmaceutics, School of Pharmaceutical Sciences, Peking University, Beijing 100191, China.

Tel.: +8610-82805937 Fax: +8610-82805937

E-mail address: luwei_pk@bjmu.edu.cn

Number of text pages: 45

Number of tables: 3

Number of figures: 10

Number of references: 48

Number of words in the Abstract: 247

Number of words in the Introduction: 757

Number of words in the Discussion: 1435

JPET Fast Forward. Published on October 30, 2017 as DOI: 10.1124/jpet.117.243931
This article has not been copyedited and formatted. The final version may differ from this version.

Nonstandard abbreviations used:

Cab, cabozantinib; Doc, docetaxel; FOCEI, first order conditional estimation with interaction; NONMEM, Non-Linear Mixed Effect Models; OFV, objective function value; PK/PD, pharmacokinetic/pharmacodynamic; TGI, tumor growth inhibition; VPC, visual predictive check.

Section assignment: Chemotherapy, Antibiotics, and Gene Therapy

Abstract

In this work, a semi-mechanistic pharmacokinetic/pharmacodynamic (PK/PD) model to quantitatively describe the antitumor activity of docetaxel (Doc) and cabozantinib (Cab) under monotherapy, concurrent therapy, interval therapy and different sequential therapy in mouse xenograft models of castration-resistant prostate cancer (CRPC) was developed and evaluated. Pharmacokinetics of Doc and Cab when administered separately and simultaneously were investigated in nude mice, and pharmacodynamic study was conducted in tumor-bearing mice treated with different dosing schedules. The PK interaction between Doc and Cab was expressed by adding the effect of Cab on the clearance of Doc in PK model. And the PD interaction between the two drugs was demonstrated by the developed PK/PD model through combination index "φ". Our results showed that the concurrent therapy and Doc followed by Cab (Doc ~ Cab) sequential therapy exhibited better tumor inhibitory efficacy than monotherapy. The Cab followed by Doc (Cab ~ Doc) sequential schedule was less effective than monotherapy, and the interval therapy did not enhance the anti-tumor efficacy compared with the concurrent therapy. Parameter "φ" estimated from the PK/PD model quantitatively characterized the action between Doc and Cab. There was no significant PD interaction between Doc and Cab in both concurrent schedule and interval schedule, while the effect of the two drugs in "Doc ~ Cab" and "Cab ~ Doc" sequential schedule was synergistic and antagonistic, respectively. The proposed model properly described the anti-tumor effects of Doc and Cab under different treatment schedules, and could be used for dose optimization through model-based simulation.

JPET Fast Forward. Published on October 30, 2017 as DOI: 10.1124/jpet.117.243931
This article has not been copyedited and formatted. The final version may differ from this version.

Introduction

Prostate cancer has the second highest incidence rate among males worldwide (Torre et al., 2016). Although advanced prostate cancer usually responds to anti-androgen therapies initially, resistance inevitably develops, leading to the emergence of castration-resistant prostate cancer (CRPC). Docetaxel (Taxotere, Doc) is a semi-synthetic taxane microtubule inhibitor, and docetaxel plus prednisone has been the standard first-line chemotherapy in patients with CRPC (McKeage, 2012). Cabozantinib (XL184, Cab) is an orally bioavailable multi-target tyrosine kinase inhibitor (TKI) with activity primarily against MET and vascular endothelial growth factor receptor 2 (VEGFR2) (Grüllich, 2014). The inhibition of MET and VEGFR2 subsequently down-regulates a series of down-stream signaling pathways, which then inhibit cell proliferation and angiogenesis. It has been reported that Cab demonstrated responses in soft tissue, visceral disease, and bone metastases in CRPC (Vaishampayan, 2014). Although two recently presented phase III trials (COMET-1 and COMET-2) evaluating Cab in CRPC did not meet their primary end points (Basch et al., 2015; Smith et al., 2015), this targeted strategy still seems to be a promising area of prostate cancer research (Modena et al., 2016).

Achieving better antitumor efficacy by drug combination is a mainstay in oncology. However, the combination of cytotoxic and anti-angiogenic drugs might be not a simple synergy. For example, the pharmacological effect of combination therapy is not better than chemotherapy alone in four large randomized clinical trials in non-small cell lung cancer (Gatzemeier et al., 2007; Herbst et al., 2004; Herbst et al., 2005; Manegold et

al., 2005). To explore the clinical failure of erlotinib and gemcitabine combination, Li (Li et al., 2013) et al. found in preclinical research that the antitumor effect of erlotinib and gemcitabine interval group was significantly different from the concurrent group. In recent years, sequential therapy has drawn increasing attention in the process of optimizing dosing regimen in cancer therapy. In preclinical, sequential treatment has been reported to augment the anti-tumor efficacy of monotherapy (Wang et al., 2015). Moreover, several clinical studies showed that sequential therapy had advantage of improving survival (Moebus et al., 2010; Signorelli et al., 2015), reducing drug resistance (Buzdar et al., 2003), and exhibiting less toxicity compared with concurrent therapy (Fornier et al., 2001).

Pharmacokinetic/pharmacodynamic (PK/PD) modeling is a good way to explore the time course relationship between drug behaviors and effects, and has become a key tool in the whole course of oncologic drug development (Manolis et al., 2013; Milligan et al., 2013). A couple of modeling approaches have been proposed to study the anti-tumor activity of drugs. These models not only can provide time-dependent quantitative estimates of the antitumor effect of a single compound (Simeoni et al., 2004), but also are capable of studying the interaction between co-administered drugs (Earp et al., 2004; Koch et al., 2009). They are also indicated as possible suitable tools for translating from preclinical to clinical occasions (Eigenmann et al., 2016; Rocchetti et al., 2007; Simeoni et al., 2013). Among these models, a linear tumor growth inhibition (TGI) model proposed earlier by Simeoni (Simeoniet al., 2004) is the most popular one. However, despite its simplicity and flexibility, the linear TGI model based on a cell-killing

hypothesis may not be able to capture the modes of action of angiogenesis inhibitors. Taking into account tumor angiogenesis, a semi-mechanistic model describing the effects of pazopanib was proposed by Ouerdani et al (Ouerdani et al., 2015). The model supposed that the tumor, through proangiogenic factors such as VEGF, was capable of extending its carrying capacity, i.e. the maximal tumor volume or mass supported by the current level of tumor vascularization. This model was developed using experimental data obtained from mice and then applied to the description of the effect of pazopanib in patients. More recently, in a study conducted to investigate the combination efficacy of bevacizumab and paclitaxel in the treatment of breast cancer in tumor bearing mice, a mathematical model was developed to describe the antiangiogenic effect of bevacizumab on tumor vasculature, which was divided into two compartments: a stable one and an unstable one (Mollard et al., 2017). Nevertheless, this model put forward higher requirements on data while explained more specific mechanisms.

The aim of this study was to develop a semi-mechanistic PK/PD model to quantitatively describe the anti-tumor effects of Doc and Cab under monotherapy, concurrent treatment schedule, interval treatment schedule and different sequential treatment schedules, using 22Rv1 and PC3 derived nude mouse xenograft models, thus to select the optimal regimen based on the results and simulations. This study may provide helpful suggestions for the combination use of Doc and Cab in clinical treatment of CRPC.

Materials and Methods

Drugs and Reagents

Doc and Cab were purchased from Melone Pharmaceutical (Dalian, China). RPMI 1640 was bought from Macgene Biotech Company, Ltd. (Beijing, China), and fetal bovine serum (FBS) was obtained from Gibco (Grand Island, New York, USA). Matrigel was purchased from Becton, Dickinson and Company (New Jersey, USA). And chromatographic grade acetonitrile and methanol were bought from Sigma (St. Louis, MO, USA).

Cell Culture and Animals

The human prostate cancer cell line 22Rv1 was purchased from Shanghai Institutes for Biological Sciences of the Chinese Academy of Sciences, and cultured in RPMI 1640 medium containing 10% FBS and antibiotic (penicillin 100 UI/ml and streptomycin 100 μg/ml). Human PC-3 prostate cancer cell line was kindly provided by Instructor Yan Song (School of Pharmaceutical Sciences, Peking University) and grown in RPMI 1640 medium containing 10% FBS. Cells were maintained at 37°C in a humidified atmosphere containing 5% CO_2.

Male nu/nu nude mice (5-week-old, 17-20g) were purchased from the Experimental Animal Center, Peking University Health Science Center (Beijing, China). The animals were housed in an environmentally controlled breeding room with specific pathogen-free condition (21°C with 50%-60% relative humidity and a 12 h light/12 h dark cycle). All animal studies were approved by the Institutional Animal Care and Use Committee.

In Vitro Cell Inhibition Assay

The sulforhodamine B (SRB) colorimetric assay (Vichai et al., 2006) was used to evaluate the growth inhibitory activity of drugs at various concentrations. Exponentially growing 22Rv1 and PC3 cells were seeded in 96-well plastic plates at a density of 2×10^4 cells/well and 4×10^3 cells/well respectively. Cells were incubated for 24 h to allow sufficient cell adhesion, and were treated with serial dilutions of Doc or Cab alone for 48 h respectively in 6 replicated wells for each drug concentration. The IC_{50} value represents the concentration resulting in 50% cell growth inhibition after a 48 h exposure to drug compared with untreated control cells, and it was calculated using GraphPad Prism 5.0 software. Then, the concentrations of Doc and Cab near the IC_{30} values were used for combination treatment study considering the balance between efficacy and toxicity (Oliveras-Ferraros et al., 2008). The treatment schedules were shown in Fig. 1A.

Pharmacokinetic Study

The mice were divided into 3 groups for Doc short-term pharmacokinetic study, Cab long-term pharmacokinetic study, and pharmacokinetic study of Doc and Cab for long-term combination. (a) For Doc short-term pharmacokinetic study, mice were injected via tail vein at a single dose of 20 mg/kg Doc (dissolved in a 90/5/5 (v/v/v) ratio, 0.9% sodium chloride/polysorbate 80/dehydrated alcohol), and blood samples were collected at 5 min, 15 min, 30 min, 1 h, 2 h, 4 h, 8 h and 12 h after administration. (b) The mice for Cab long-term pharmacokinetic study were given Cab (formulated in water) at a dose of 10 mg/kg/day by oral gavage, and blood samples were collected at 5 min, 15

min, 30 min, 1 h, 2 h, 4 h, 8 h, 12 h, 72 h, 168 h and 288 h after the first dose. (c) The mice for Doc and Cab combination pharmacokinetic study were administered Doc at a dose of 20 mg/kg/week and Cab at a dose of 10 mg/kg/day. The experiment lasted for 12 days, and at day 1 and day 8 Doc and Cab were administered simultaneously. Blood samples were collected at 5 min, 15 min, 30 min, 1 h, 2 h, 4 h, 8 h, 12 h, 72 h, 168 h and 288 h after the first dose. All the blood samples were centrifugated at 4,000 rpm for 10 min, then the upper plasma was collected and stored at −80°C before analysis. The animals were euthanized after sampling.

The quantification of Doc and Cab was monitored using an API4000 QTRAP Mass Spectrometer (Applied Biosystems Inc., USA) equipped with an electrospray ionization (ESI) source system, and controlled by AnalystTM Version 1.6. Chromatographic separation was performed on a DIONEX UltiMate 3000 UHPLC system. Doc was separated by an Ultimate C-18 column (3.0 × 50mm i.d., 3 μm particle size; Waters Corp., Milford, MA, USA) using an isocratic mobile phase (pure water containing 1 mM ammonium formate:acetonitrile=45:55, v/v) at room temperature. The ion transitions monitored was from m/z 808.5→527.4; the ionspray voltage was kept at 5 kV, and the temperature was 300°C. The flow rate was 0.4 ml/min and the overall run time was 4 min, with a quantitative range of 5-1500 ng/ml. The high performance liquid chromatography-tandem mass spectrometry (HPLC-MS/MS) method was validated in accordance with the Guidance for Industry, Bioanalytical Method Validation, as specified by FDA (FDA, 2013). The concentration of Cab was determined by a LC-MS/MS method previously developed by our group (Su et al., 2015). Separation of Cab

was achieved on a reversed phase C18 column (50 × 2 mm, 5 μm) at ambient temperature using isocratic elution with acetonitrile-water (45:55, v/v) containing 5 mM ammonium formate buffer (finally adjusted to apparent pH* = 5.0 with formic acid). The flow rate was 0.4 mL/min. Calibration curve was linear ($r > 0.99$) in a concentration range of 0.5–1000 ng/mL.

In Vivo Pharmacodynamic Study

22Rv1 and PC3 tumor-bearing mice were used for pharmacodynamic study. Both xenograft models were used to investigate and compare the anticancer efficacy of monotherapy, concurrent therapy, interval therapy, and sequential therapy of the two drugs. The various treatment groups were shown in Table 1, and the schematic diagram of treatment schedules was represented in Supplementary Fig. S1.

Firstly, we established the 22Rv1-inoculated xenograft model. Briefly, 5×10^6 22Rv1 cells were suspended in 100 μL mixed solution of RPMI 1640 free of FBS and matrigel (v/v=1/1), and inoculated subcutaneously into mouse's right flank. Tumor diameter was measured by vernier caliper and converted to tumor volume using the formula: TV (mm^3) = length × $width^2$ × 0.5. When tumor volumes reached 100-200 mm^3, mice were randomly assigned to 9 different treatment groups (n=5~6 in each group): (1) vehicle control; (2) Doc 5; (3) Doc 10; (4) Cab 10; (5) Doc 5 + Cab 10; (6) Doc 10 + Cab 10; (7) Doc 5 6h Cab 10; (8) Doc 10 6h Cab 10; (9) Doc 10 ~ Cab 10. Treatments lasted for 3 weeks, and the tumor size and body weight in various groups were recorded every two days. The percent tumor growth inhibition (%TGI) was determined as the average change in vehicle treated tumors (ΔVehicle) minus the average change in test agents

treated tumors (ΔTreated) divided by ΔVehicle and expressed as a percentage (Huck et al., 2014) (Eq.1). Because %TGI is a time-dependent efficacy endpoint, it is calculated at a fixed time point. In our study, %TGI was calculated at the end of the dosing period.

$$\%TGI = \frac{(Control_{tday} - Control_{0day}) - (Tteated_{tday} - Treated_{0day})}{Control_{tday} - Control_{0day}} \times 100\% \quad (1)$$

We then established the PC3 xenograft model. Similarly, 5×10^6 PC3 cells were suspended in 100 μL mixed solution of RPMI 1640 free of FBS, and inoculated subcutaneously into mouse's right flank. Mice were randomly assigned to 7 different treatment groups (n=5~6 each group): (1) vehicle control; (2) Doc 5; (3) Cab 10; (4) Doc 5 + Cab 10; (5) Doc 5 6h Cab 10; (6) Doc 5 ~ Cab 10; (7) Cab 10 ~ Doc 5. Treatments were conducted for 4 weeks and the tumor size and body weight were recorded as mentioned above.

PK/PD models

The experimental data were modeled using the First Order Conditional Estimation with Interaction (FOCEI) method with NONMEM 7.2 (ICON, MD, USA). The block diagram of the entire model is shown in Fig. 2.

PK model

The Doc concentration-time curve was estimated using a two-compartment model, while the PK profile of Cab was described by a one-compartment model with first-order absorption. In our study, since Doc was injected once a week while Cab was administered by oral gavage every day, we assumed that Doc had no effect on Cab PK during PK/PD modeling process. At the same time, we used the log-likelihood ratio test to evaluate the effect of Cab on the PK profile of Doc. As a result, for mice taking both

Doc and Cab, Doc clearance (CL) was adjusted by the influence of Cab plasma concentration (Eq. 2). In this equation, CL_c and CL_s represent Doc clearance of mice taking both drugs and single Doc, respectively; $IC50_{Cab}$ represents the concentration of Cab causing half of maximum impact on Doc CL; C_{Cab} is the concentration of Cab in mouse plasma.

$$CL_c = CL_s \cdot (1 - \frac{C_{Cab}}{IC50_{Cab} + C_{Cab}}) \quad (2)$$

PK/PD model

A logistic tumor growth model was used as the base model for tumor natural growth dynamics of 22Rv1 xenografts (Yamazaki et al., 2011). The natural growth of the tumor can be described by an exponential phase with a self-limitation, eventually reaching a plateau. The growth rate of tumor can be described by Eq. 3,

$$\frac{dX(t)}{dt} = k_{ng} \cdot X(t) \cdot \left(1 - \frac{X(t)}{KP}\right),\ Xt(0) = V(0) \quad (3)$$

where X(t) represents the volume of proliferating tumor cells at time t, k_{ng} is the constant net growth rate, and KP represents the tumor carrying capacity (the maximum sustainable tumor volume), which is assumed to be limited by nutrition supplied through vasculature as well as the growth space in tumor (Yamazaki et al., 2011).

In Doc monotherapy groups, it is assumed that chemotherapy makes some cells non-proliferating and eventually brings them to death through a mortality chain (Simeoni et al., 2004). A transit compartment model has been used to characterize the time delay between drug exposure and drug effect; the portion of proliferating cells within the total tumor volume is denoted as X1, and k1 is the constant transit rate between non-

proliferating compartments (X2, X3, X4). X(t) is the total volume of the cells in various stages. The rate from proliferating to non-proliferating cells is in proportion with Doc concentration in plasma (C_{Doc}), with a cofficient of k_{Doc} which describes its anti-tumor potency. The differential equations are as follows:

$$\frac{dX1}{dt} = k_{ng} \cdot X1 \cdot \left(1 - \frac{X(t)}{KP}\right) - k_{Doc} \cdot C_{Doc} \cdot X1,\ X1(0) = V(0) \quad (4)$$

$$\frac{dX2}{dt} = k_{Doc} \cdot C_{Doc} \cdot X1 - k1 \cdot X2,\ X2(0) = 0 \quad (5)$$

$$\frac{dX3}{dt} = k1 \cdot (X2 - X3),\ X3(0) = 0 \quad (6)$$

$$\frac{dX4}{dt} = k1 \cdot (X3 - X4),\ X4(0) = 0 \quad (7)$$

$$X(t) = X1 + X2 + X3 + X4 \quad (8)$$

In Cab treatment groups, as Cab is a receptor tyrosine kinase inhibitor with activity against MET and VEGFR2 (Grüllich, 2014), hence blocking nutrition supply of the tumor, we accordingly assumed that Cab exerted inhibitory effect on KP (Ouerdani et al., 2015) instead of damaging tumor cells (Eq. 9). In this equation, the concentration of Cab causing half of maximum inhibition was represented by $EC50_{Cab}$.

$$\frac{dX(t)}{dt} = k_{ng} \cdot X(t) \cdot \left(1 - \frac{X(t)}{KP \cdot \left(1 - \frac{C_{Cab}}{EC50_{Cab} + C_{Cab}}\right)}\right), \quad Xt(0) = V(0) \quad (9)$$

In the drug combination groups, combination index "φ" was introduced to k_{Doc} to determine the interaction of Doc and Cab on tumor growth. The φ value greater or less than 1 signifies the degree of increase or decrease in antitumor effect. Therefore, parameter φ can indicate synergism or antagonism of the two drugs. The equation is

shown as Eq.10.

$$\frac{dX1}{dt} = k_{ng} \cdot X1 \cdot \left(1 - \frac{X(t)}{KP \cdot \left(1 - \frac{C_{Cab}}{EC50_{Cab} + C_{Cab}}\right)}\right) - \varphi \cdot k_{Doc} \cdot C_{Doc} \cdot X1,\ X1(0) = V(0) \quad (10)$$

Gompertz model (Laird, 1964) was used for fitting the tumor natural growth of PC3 xenografts (Eq.11), in which k_{ng} is the constant net growth rate, and Nss represents the maximum sustainable tumor volume. Similarly, Doc exhibited a linear-killing effect on cell growth (Eq. 12) and Cab affected Nss (Eq. 13). For combination groups, φ of "Doc + Cab" group, "Doc 6h Cab" group, "Doc ~ Cab" group and "Cab ~ Doc" group was represented by φ_1, φ_2, φ_3 and φ_4, respectively (Eq. 14).

$$\frac{\mathrm{dX(t)}}{\mathrm{dt}} = k_{ng} \cdot \mathrm{X(t)} \cdot \mathrm{Ln}\left(\frac{Nss}{X(t)}\right),\ \mathrm{Xt(0)} = \mathrm{V(0)} \quad (11)$$

$$\frac{dX1}{dt} = k_{ng} \cdot X1 \cdot \mathrm{Ln}\left(\frac{Nss}{X(t)}\right) - k_{Doc} \cdot C_{Doc} \cdot X1,\ X1(0) = V(0) \quad (12)$$

$$\frac{\mathrm{dX(t)}}{\mathrm{dt}} = k_{ng} \cdot \mathrm{X(t)} \cdot \mathrm{Ln}\left(\frac{Nss \cdot \left(1 - \frac{C_{Cab}}{EC50_{Cab} + C_{Cab}}\right)}{X(t)}\right),\ \mathrm{Xt(0)} = \mathrm{V(0)} \quad (13)$$

$$\frac{\mathrm{dX1}}{\mathrm{dt}} = k_{ng} \cdot \mathrm{X1} \cdot \mathrm{Ln}\left(\frac{Nss \cdot \left(1 - \frac{C_{Cab}}{EC50_{Cab} + C_{Cab}}\right)}{X(t)}\right) - \varphi \cdot k_{Doc} \cdot C_{Doc} \cdot X1,\ X1(0) = V(0) \quad (14)$$

Model selection was based on NONMEM objective function value (OFV), parameter estimates, relative standard errors (RSE) in the estimate, and exploratory analysis of the goodness-of-fit (GOF) plots. Model validations were performed by visual predictive check (VPC) of the predictions with 1000 simulations using Perl speaks NONMEM (PsN, Version 3.5.3).

Data Analysis and Model Simulations

The results of PD study in vivo were presented as mean ± SD by the GraphPad Prism 5.0 software. Student's t-test was used to determine the significance among the groups, and difference at a level of $p < 0.05$ was considered statistically significant.

The tumor growth profiles of mice bearing 22Rv1 and PC3 xenograft under concurrent and "Doc ~ Cab" sequential treatment with different dose combinations were simulated from day 0 to day 28. The model parameters obtained from the PK/PD model were fixed and the initial tumor volume was set to 160 mm^3. The doses of Doc used for simulation were "0, 2, 4, 6, 8, 10, 12 mg/kg/week" and "0, 2, 4, 6, 8, 10 mg/kg/week" on 22Rv1 tumor-bearing mice and PC3 tumor-bearing mice respectively. Accordingly, the doses of Cab for simulation were "0, 2, 4, 6, 8, 10, 12 mg/kg/day" and "0, 2.5, 5, 7.5, 10, 12.5, 15, 20 mg/kg/day" on 22Rv1 tumor-bearing mice and PC3 tumor-bearing mice respectively. The doses of Doc and Cab for simulations were selected on the grounds that the %TGI was between 15% and 85% for monotherapy in each model. Furthermore, kinetic tumor volume data were converted to %TGI using Eq. 1, and %TGI of different combination schedules on day 28 was presented in form of response surface.

Results

In Vitro Cell Inhibition

The cell inhibition effects of Doc and Cab were found to be dose-dependent in both 22Rv1 and PC3 cells according to our study. The IC_{50} values of Doc were 9.86 nM and 4.95 nM for 22Rv1 and PC3 cells respectively, and those of Cab were 13.54 μM and 12.80 μM for 22Rv1 and PC3 cells respectively. The concentrations of Doc and Cab used for combination study were 7 nM and 7.3 μM for 22Rv1 cells respectively, and 2.5 nM and 9 μM for PC3 cells respectively, which were approximate to their IC_{30} values. The results were shown in Fig. 1B. Concurrent treatment and "Doc ~ Cab" sequential treatment were more effective in inhibiting cancer cell growth than treatment with Doc or Cab alone in both cell lines. In contrast, "Cab ~ Doc" sequential treatment was less effective than "Doc ~ Cab" sequential treatment.

Pharmacokinetic study

The plasma concentration–time curves of Doc on linear and logarithmic scale after injecting single dose of 20 mg/kg Doc or administering 20 mg/kg Doc and 10 mg/kg Cab simultaneously in nude mice were shown in Fig. 3A. The mouse plasma concentration of Cab after giving 10 mg/kg/day Cab alone or 10 mg/kg/day Cab combined with 20 mg/kg/week Doc were shown in Fig. 3B. For single dose of Doc, combination of Cab showed a discrepancy after 2 h, which indicates different terminal half-life. For long-term investigation of Cab PK shown in Fig. 3B, combination of Doc once a week had no manifest influence on the concentration-time profile of Cab, nor did Cab have any self-induction or self-inhibition effect. Therefore, in the following

PK/PD modeling, we only added the influence of Cab on Doc PK (Eq. 2).

The concentration-time curve of Doc was fitted by a two-compartment model with correction on CL for concurrent treatment groups and interval treatment groups, while that of Cab was described by a one-compartment model with first-order absorption. The parameters estimated were summarized in Table 2.

In Vivo Pharmacodynamic Study

Fig. 4 showed the tumor inhibitory effects of various schedules on mice bearing 22Rv1 xenografts and the picture of excised tumors on day 21. The average %TGI of "Doc 5", "Doc 10" and "Cab 10" group at the end of treatment were 38.26%, 72.54% and 71.49%, respectively. Compared with monotherapy, drug combination groups showed increased inhibition of tumor growth, with %TGI of 88.50%, 84.93%, 100.96% and 100.59% for "Doc 5 + Cab 10", "Doc 5 6h Cab 10", "Doc 10 + Cab 10" and "Doc 10 6h Cab 10" group, respectively. The interval therapy did not enhance the anti-tumor efficacy compared with the concurrent therapy. Besides, the %TGI of "Doc10 ~ Cab 10" sequential group was 90.07%, which was higher than those of monotherapy groups. As shown in supplementary Fig. S2A-B, body weights of mice were stable during treatment, and organ coefficients (organ weight / (body weight – tumor weight) * 100%) showed no abnormality among various groups, indicating the safety of all the dosing regimens.

The tumor growth inhibition under different dosing regimens in mice bearing PC3 xenograft was shown in Fig.5. The inhibition ratios compared with control groups were 62.10% and 33.87% in "Doc 5" and "Cab 10" monotherapy groups, respectively, as

well as 88.92%, 86.72%, 74.48%, and 30.76% in “Doc 5 + Cab 10”, “Doc 5 6h Cab 10”, “Doc 5 ~ Cab 10”, and “Cab 10 ~ Doc 5” groups, respectively. Being consistent with the results from 22Rv1 model, the concurrent group exerted lower tumor burden than all monotherapy groups, and the anti-tumor efficacy in the interval group was similar to that in the concurrent group. In addition, the tumor growth inhibition in two sequential groups exhibited obvious contrary patterns. Compared with all monotherapy groups, the tumor burden was lower in “Doc 5 ~ Cab 10” sequential group but higher in “Cab 10 ~ Doc 5” group. The mouse body weight during treatment and organ coefficients among various groups were shown in supplementary Fig. S2C-D.

PK/PD Model

The estimated PK model parameters were listed in Table 2. And the visual predictive check (VPC) results and GOF plots of PK models were presented in Fig. 6 and supplementary Fig. S3, respectively.

Tumor volume data were fitted using sequential fitting method to eliminate the confounding effects in the estimation of drug efficacy parameters and φ. Tumor growth data of control group were fitted at the first step, and then growth parameters obtained were fixed in the subsequent fitting process. The combination index “φ” was estimated by fixing the inherent drug efficacy parameters obtained from the modeling of monotherapy groups. The parameters estimated were summarized in Table 3, and the VPC results stratified by group were presented in Fig. 7 and Fig. 8 for 22Rv1 and PC3 xenograft model, respectively. The combination indexes obtained from PK/PD models were compared in Fig. 9.

Obtained from the 22Rv1 PK/PD model, φ values of the concurrent group and the interval group were 0.98 ± 0.21 (95% confidence interval) and 1.19 ± 0.26 respectively, and 1 was within their 95% confidence interval, indicating that Doc and Cab had no significant PD interaction under both treatment schedules. However, φ obtained from "Doc ~ Cab" group was 2.09 ± 0.74, which was higher than 1 as well as that of the concurrent and interval schedule, indicating synergy of the two drugs in "Doc ~ Cab" sequential treatment.

For PC3 xenograft model, the combination indexes of concurrent group, interval group, "Doc ~ Cab" and "Cab ~ Doc" sequential group were 1.25 ± 0.25, 1.34 ± 0.34, 3.63 ± 1.35 and 0.54 ± 0.22, respectively. These results suggested that Doc and Cab exhibited similar effect under concurrent schedule and interval schedule, since most of their 95% confidence interval were overlapped. Moreover, "Doc ~ Cab" sequential schedule showed synergy of Doc and Cab because φ is much greater than 1, which was consistent with the results from 22Rv1 PK/PD model. However, "Cab ~ Doc" sequential group exhibited antagonism indicated by φ, whose value was less than 1.

Model Simulations

Simulations were performed on concurrent schedule and "Doc ~ Cab" sequential schedule in this study since the experimental data demonstrated the enhanced anti-tumor effect in the concurrent groups and the PK/PD model parameter φ confirmed the highest synergy of the two drugs in "Doc ~ Cab" sequential groups. Besides, concurrent schedule is more convenient and acceptable than the interval one in medical practice, although there was no significant difference in the anti-tumor effect between them.

JPET Fast Forward. Published on October 30, 2017 as DOI: 10.1124/jpet.117.243931
This article has not been copyedited and formatted. The final version may differ from this version.

By fixing the parameters obtained from 22Rv1 PK/PD model, simulated response surface of %TGI on day 28 under different dose combinations were shown in Fig. 10A-B. For "Doc + Cab" concurrent schedule, Doc combined with Cab showed enhanced tumor inhibition compared with Doc or Cab monotherapy. It should be noticed that under the concurrent treatment, a low dose of Cab could increase the total anti-cancer effect dramatically, which can be seen from the steepness of the surface along the y-axis. For example, the %TGI under the treatment of 6 mg/kg/week Doc was 47.3%, while the %TGI of "Doc 6 + Cab 2" rose to 68.6%. However, for the "Doc ~ Cab" sequential schedule, low dose of Doc (2 mg/kg/week) combined with Cab showed no benefit compared with Cab monotherapy, but when the dose of Doc was higher than 4 mg/kg/week, sequential treatment was obviously superior to monotherapy of both two drugs.

Simulated %TGI based on the PC3 PK/PD model on day 28 was shown in Fig. 10C-D. Both the concurrent and sequential treatment exhibited obvious advantage over monotherapy. For both concurrent and "Doc ~ Cab" sequential schedule, Doc combined with a low dose of Cab could increase the total anti-cancer effect dramatically. Subsequently, the %TGI increased modestly with the increasing dose of Cab, given the same dose of Doc. For instance, the %TGI was 59.3% for 6 mg/kg/week Doc treatment and 14.0% for monotherapy of 2.5 mg/kg/day Cab, while the %TGI of "Doc 6 + Cab 2.5" and "Doc 6 ~ Cab 2.5" were 80.0% and 79.5% respectively. However, when the dose of Cab increased to 5 mg/kg/day, the %TGI only rose to 87.3% and 80.9% for "Doc 6 + Cab 5" and "Doc 6 ~ Cab 5" respectively.

Discussion

In this study on male nude mice bearing 22Rv1 and PC3 xenografts, a semi-mechanistic PK/PD model with PK interaction, which well characterized the quantitative relationship between plasma concentration and tumor progression in various regimens of Doc combined with Cab, was developed for the first time. Simulations-based evaluation showed that the model performed well in all treatment schedules.

For docetaxel, a cytotoxic agent, the responses to treatment were consistent in vitro and in vivo in both xenograft models, which can be seen from the IC_{50} (9.86 nM and 4.95 nM for 22Rv1 and PC3 cells respectively) in vitro and the anti-tumor effect coefficient k_{Doc} in two xenograft models (0.000206 for 22Rv1 and 0.000289 for PC3 xenografts). The IC_{50} values of Cab in the two cell lines were approximate (13.54 μM and 12.80 μM for 22Rv1 and PC3 cells respectively), suggesting its cytotoxic effect on both cells is similar and weak. However, a more than 5-fold difference of EC50 estimated from PK/PD model in two xenograft models (399 μg/L for PC3 vs 2210 μg/L for 22Rv1 respectively) was noticed. As a multi-targeted TKI, Cab exhibits strong inhibition on phosphorylation of tyrosine kinase receptor and corresponding downstream signaling pathways. The difference of EC50 means Cab exhibits stronger inhibition on phosphorylation of tyrosine kinase receptor in 22Rv1 xenograft model than that in PC3 xenograft model. This may be due to different origins and cell-type specific characteristics (Wu et al., 2013) as well as the different tumor microenvironment in the two xenograft models. In addition, recent observation indicated that PC3 cell line is more characteristic of prostatic small cell neuroendocrine carcinoma rather than

adenocarcinoma (Tai et al., 2011), so the results of PC3 PK/PD model may have more reference value in small cell carcinoma patients.

The “Cab ~ Doc” sequential schedule was less effective than the “Doc ~ Cab” sequential schedule both in vitro and in vivo, which may be explained by different effects of the two drugs on cell cycle arrest (Pan et al., 2011). As an anti-microtubule agent, Doc stabilizes microtubule during cell division and causes cell cycle arrest in G2/M phase (Bissery, 1995). However, Cab has been reported to affect G0/G1 phase of cell cycle (Lu et al., 2016). When Cab was given first, cells were arrested in G0/G1 phase, leading to the reduction in the proportion of cells in G2/M phase, thus may affect the effect of Doc subsequently. Therefore, the “Cab ~ Doc” sequential regimen was less effective. Similar findings of schedule-dependent interaction have been reported by several teams (Jiang et al., 2014; Pan et al., 2011; Ricotti et al., 2003; Tamatani et al., 2012; Wang et al., 2012).

Our in vivo experimental results showed the anti-tumor effect of “Doc + Cab” concurrent therapy was better than that of “Doc ~ Cab” sequential therapy, while the values of φ in the latter treatment groups were much higher than that in the former groups (2.09 vs 0.98, and 3.63 vs 1.25 in 22Rv1 and PC3 xenograft model, respectively). This is because the total doses of the two schedules were different. For a duration of two weeks, the mice in “Doc 5 ~ Cab 10” group were administered 5 mg/kg Doc and 10*7 mg/kg Cab, while the mice in “Doc 5 + Cab 10” group were administered 5*2 mg/kg Doc and 10*14 mg/kg Cab. The total dose in the concurrent group was twice of that in the sequential group in two weeks, leading to smaller tumor size in “Doc 5 +

Cab 10" group. As higher φ value means greater synergy of PD interaction, φ value estimated from the concurrent schedule showed no significant PD interaction of the two drugs since the value of φ was close to 1, while that of the "Doc ~ Cab" sequential therapy showed synergy of the two drugs. These results suggest that "Doc ~ Cab" sequential treatment could be a promising therapeutic strategy for prostate cancer treatment considering long-term drug resistance or toxicity.

Doc and Cab are both substrates of CYP3A4 enzyme (Engels et al., 2005; Nguyen et al., 2015), therefore, it is necessary to investigate the PK interaction between them when they are used in combination. Based on the data from our PK studies, for mice administered Doc and Cab simultaneously, the AUC_{0-12} of Doc increased by 30% compared with that when Doc was administered alone, suggesting the likelyhood of PK interaction between Doc and Cab. We further investigated this possible PK interaction using population approach. We considered monotherapy vs combination treatment as binary covariate (E_com, 0 for monotherapy, otherwise to be estimated for combination treatment) and used the log-likelihood ratio test to evaluate the significance of E_com. The inclusion of E_com on Doc CL caused a significant decrease of OFV (-22.4, $p<0.001$). Similarly, we investigated the effect of Doc on Cab PK, and the results showed that the inclusion of E_com on CL or V of Cab did not significantly decrease OFV. These results were in agreement with our speculation. Because Cab was administered every day while Doc was given once a week, the effect of Doc on Cab PK could be neglected during the modeling process. Thus, we added the PK interaction only for Doc in PK/PD model and finally used Eq. 2 to describe the effect of Cab on

JPET Fast Forward. Published on October 30, 2017 as DOI: 10.1124/jpet.117.243931
This article has not been copyedited and formatted. The final version may differ from this version.

Doc CL. We have compared the parameters estimated with or without PK interaction (supplementary Table. S1 and Table. S2). The values of φ estimated from the model without PK interaction were higher than those with PK interaction in the concurrent and interval schedules, indicating that part of PD interaction of the two drugs was interpreted by PK interaction, especially in the concurrent schedule.

Since Cab is an angiogenesis inhibitor rather than a cytotoxic agent, our model took into account the role of tumor vasculature in tumor growth and shrinkage. In the modeling process, the model with Cab having both cytotoxic and antiangiogenic effects have been tested. We found that the plasma concentration of Cab had almost no impact on cytotoxicity (k_{Cab} was initially estimated at 0.0000001) while that on angiogenesis was significant ($EC50_{Cab}$, estimated at 399 μg/L and 2210 μg/L for 22Rv1 and PC3 model respectively). Therefore, in our model structure, the effect of Cab was assumed on the tumor carrying capacity KP (or Nss) only, although both cytotoxicity and anti-angiogenesis of Cab had been reported by Ouerdani et al. (Ouerdani et al., 2015). It may be due to the relatively low dose of Cab in our study (Bentzien et al., 2013; Yakes et al., 2011), which cannot cause significant cell-killing effect directly.

To determine the dosing regimens of both drugs, we referenced those in clinic treatment. The standard dose of Doc for patients with CRPC is 75 mg/m^2/three weeks, and the equivalent dose in mice is about 18 mg/kg/three weeks according to body surface area, which means 6 mg/kg/week in mice equivalently. The simulated %TGI for both 22Rv1 and PC3 tumor bearing mice on day 28 under the treatment of 6 mg/kg/week Doc could be augmented notably when combined with a low dose of Cab (2 or 2.5 mg/kg/day,

equivalent to 15-20 mg/day in human), especially in PC3 xenograft model. It can be seen from Fig. 10C-D that the %TGI was 59.3% for Doc 6 mg/kg/week monotherapy, while the %TGI of "Doc 6 + Cab 2.5" and "Doc 6 ~ Cab 2.5" were 80% and 79.5% respectively. Notably, it has been reported that compared with the 140 mg daily dose of Cab used in thyroid cancer, lower doses of 60 mg and 40 mg daily in prostate cancer phase II studies demonstrated lower toxicity without compromising efficacy (Lee et al., 2013; Vaishampayan, 2014). Therefore, small dose of Cab may enhance efficacy when combined with Doc in the treatment of CRPC.

In summary, the proposed PK/PD model quantitatively described the relationship between the plasma concentration and the anticancer efficacy of Doc and Cab in different schedules for the treatment of CRPC in mice. However, the developed model was not able to make simulations apart from the experimental schedules since the parameter φ was empirical and varied among schedules. The current model need to be further optimized after we get more mechanistic data in the future. In our study, concurrent treatment of Doc and Cab showed better tumor inhibitory efficacy than monotherapy, the "Doc ~ Cab" sequential schedule was superior to monotherapy while the "Cab ~ Doc" sequential schedule was less effective. PK/PD modeling results indicated that the two drugs exhibited optimal synergy under the "Doc ~ Cab" sequential schedule. The developed PK/PD model may provide reference for the rational use of chemotherapeutic drugs in combination with anti-angiogenic agents.

Acknowledgements

We sincerely appreciate Dr. Jun Li's (State Key Laboratory of Natural and Biomimetic Drugs, Peking University) kind help during the development of LC–MS/MS analysis method of docetaxel.

Authorship Contributions

Participated in research design: WJ Chen, L Li, Zhou, Lu

Conducted experiments: WJ Chen, J Li, Yang, Su, Yao

Performed data analysis: WJ Chen, R Chen, Fu

Wrote or contributed to the writing of the manuscript: WJ Chen, Zhou, Lu

References

Basch EM, Scholz MC, De Bono JS, Vogelzang NJ, De Souza PL, Marx GM, Vaishampayan UN, George S, Schwarz JK, and Antonarakis ES (2015) Final analysis of COMET-2: Cabozantinib (Cabo) versus mitoxantrone/prednisone (MP) in metastatic castration-resistant prostate cancer (mCRPC) patients (pts) with moderate to severe pain who were previously treated with docetaxel (D) and abiraterone (A) and/or enzalutamide (E). Journal of Clinical Oncology 33: 7_suppl, 141.

Bentzien F, Zuzow M, Heald N, Gibson A, Shi Y, Goon L, Yu P, Engst S, Zhang W, Huang D, Zhao L, Vysotskaia V, Chu F, Bautista R, Cancilla B, Lamb P, Joly AH, and Yakes FM (2013) In vitro and in vivo activity of cabozantinib (XL184), an inhibitor of RET, MET, and VEGFR2, in a model of medullary thyroid cancer. Thyroid : official journal of the American Thyroid Association 23(12): 1569-1577.

Bissery MC (1995) Preclinical pharmacology of docetaxel. European journal of cancer 31A Suppl 4: S1-6.

Buzdar AU, and Hortobagyi GN (2003) Sequential paclitaxel reduces recurrence and mortality in women with early breast cancer. Cancer treatment reviews 29(5): 449-452.

Earp J, Krzyzanski W, Chakraborty A, Zamacona MK, and Jusko WJ (2004) Assessment of drug interactions relevant to pharmacodynamic indirect response models. J Pharmacokinet Pharmacodyn 31(5): 345-380.

Eigenmann MJ, Frances N, Hoffmann G, Lave T, and Walz AC (2016) Combining Nonclinical Experiments with Translational PKPD Modeling to Differentiate Erlotinib and Gefitinib. Mol Cancer Ther 15(12): 3110-3119.

Engels F, Sparreboom A, Mathot R, and Verweij J (2005) Potential for improvement of docetaxel-based chemotherapy: a pharmacological review. British journal of cancer 93(2): 173-177.

FDA US (2013) Guidance for Industry: Bioanalytical Method Validation. [https://www.fda.gov/downloads/drugs/guidancecomplianceregulatoryinformation/guidances/ucm368107.pdf]

Fornier MN, Seidman AD, Theodoulou M, Moynahan ME, Currie V, Moasser M, Sklarin N, Gilewski T, D'Andrea G, and Salvaggio R (2001) Doxorubicin Followed by Sequential Paclitaxel and Cyclophosphamide versus Concurrent Paclitaxel and Cyclophosphamide. Clinical cancer research 7(12): 3934-3941.

Gatzemeier U, Pluzanska A, Szczesna A, Kaukel E, Roubec J, De Rosa F, Milanowski J, Karnicka-Mlodkowski H, Pesek M, and Serwatowski P (2007) Phase III study of erlotinib in combination with cisplatin and gemcitabine in advanced non–small-cell lung cancer: The Tarceva Lung Cancer Investigation Trial. Journal of Clinical Oncology 25(12): 1545-1552.

Grüllich C (2014) Cabozantinib: a MET, RET, and VEGFR2 tyrosine kinase inhibitor. Small Molecules in Oncology pp 207-214 Springer, Berlin, Heidelberg.

Herbst RS, Giaccone G, Schiller JH, Natale RB, Miller V, Manegold C, Scagliotti G, Rosell R, Oliff I, and Reeves JA (2004) Gefitinib in combination with paclitaxel

and carboplatin in advanced non–small-cell lung cancer: A phase III trial—INTACT 2. Journal of Clinical Oncology 22(5): 785-794.

Herbst RS, Prager D, Hermann R, Fehrenbacher L, Johnson BE, Sandler A, Kris MG, Tran HT, Klein P, and Li X (2005) TRIBUTE: A phase III trial of erlotinib hydrochloride (OSI-774) combined with carboplatin and paclitaxel chemotherapy in advanced non–small-cell lung cancer. Journal of Clinical Oncology 23(25): 5892-5899.

Huck JJ, Zhang M, Mettetal J, Chakravarty A, Venkatakrishnan K, Zhou X, Kleinfield R, Hyer ML, Kannan K, and Shinde V (2014) Translational Exposure–Efficacy Modeling to Optimize the Dose and Schedule of Taxanes Combined with the Investigational Aurora A Kinase Inhibitor MLN8237 (Alisertib). Molecular cancer therapeutics 13(9): 2170-2183.

Jiang Y, Yuan Q, and Fang Q (2014) Schedule-dependent synergistic interaction between docetaxel and gefitinib in NSCLC cell lines regardless of the mutation status of EGFR and KRAS and its molecular mechanisms. Journal of cancer research and clinical oncology 140(7): 1087-1095.

Koch G, Walz A, Lahu G, and Schropp J (2009) Modeling of tumor growth and anticancer effects of combination therapy. J Pharmacokinet Pharmacodyn 36(2):179-197.

Laird AK (1964) Dynamics of tumour growth. British journal of cancer 18(3): 490.

Lee RJ, Saylor PJ, Michaelson MD, Rothenberg SM, Smas ME, Miyamoto DT, Gurski CA, Xie W, Maheswaran S, Haber DA, Goldin JG, and Smith MR (2013) A

dose-ranging study of cabozantinib in men with castration-resistant prostate cancer and bone metastases. Clinical cancer research : an official journal of the American Association for Cancer Research 19(11): 3088-3094.

Li M, Li H, Cheng X, Wang X, Li L, Zhou T, and Lu W (2013) Preclinical pharmacokinetic/pharmacodynamic models to predict schedule-dependent interaction between erlotinib and gemcitabine. Pharmaceutical research 30(5): 1400-1408.

Lu JW, Wang AN, Liao HA, Chen CY, Hou HA, Hu CY, Tien HF, Ou DL, and Lin LI (2016) Cabozantinib is selectively cytotoxic in acute myeloid leukemia cells with FLT3-internal tandem duplication (FLT3-ITD). Cancer letters 376(2): 218-225.

Manegold C, Pilz LR, Koschel G, Schott-von Römer K, Mezger J, Hruska D, Dornof W, Gosse H, and Gatzemeier U (2005) Randomized multicenter phase II study of gemcitabine versus docetaxel as first-line therapy with second-line crossover in advanced-stage non–small-cell lung cancer. Clinical lung cancer 7(3): 208-214.

Manolis E, Rohou S, Hemmings R, Salmonson T, Karlsson M, and Milligan P (2013) The role of modeling and simulation in development and registration of medicinal products: output from the EFPIA/EMA modeling and simulation workshop. CPT: pharmacometrics & systems pharmacology 2(2): 1-4.

McKeage K (2012) Docetaxel: a review of its use for the first-line treatment of advanced castration-resistant prostate cancer. Drugs 72(11): 1559-1577.

Milligan P, Brown M, Marchant B, Martin S, Van Der Graaf P, Benson N, Nucci G, Nichols D, Boyd R, and Mandema J (2013) Model-based drug development: a rational approach to efficiently accelerate drug development. Clinical Pharmacology & Therapeutics 93(6): 502-514.

Modena A, Massari F, Ciccarese C, Brunelli M, Santoni M, Montironi R, Martignoni G, and Tortora G (2016) Targeting Met and VEGFR Axis in Metastatic Castration-Resistant Prostate Cancer:'Game Over'? Targeted oncology 11(4): 431-446.

Moebus V, Jackisch C, Lueck HJ, du Bois A, Thomssen C, Kurbacher C, Kuhn W, Nitz U, Schneeweiss A, Huober J, Harbeck N, von Minckwitz G, Runnebaum IB, Hinke A, Kreienberg R, Konecny GE, and Untch M (2010) Intense dose-dense sequential chemotherapy with epirubicin, paclitaxel, and cyclophosphamide compared with conventionally scheduled chemotherapy in high-risk primary breast cancer: mature results of an AGO phase III study. Journal of clinical oncology : official journal of the American Society of Clinical Oncology 28(17): 2874-2880.

Mollard S, Ciccolini J, Imbs DC, El Cheikh R, Barbolosi D, and Benzekry S (2017) Model driven optimization of antiangiogenics + cytotoxics combination: application to breast cancer mice treated with bevacizumab + paclitaxel doublet leads to reduced tumor growth and fewer metastasis. Oncotarget 8(14): 23087-23098.

Nguyen L, Holland J, Miles D, Engel C, Benrimoh N, O'reilly T, and Lacy S (2015)

Pharmacokinetic (PK) drug interaction studies of cabozantinib: effect of CYP3A inducer rifampin and inhibitor ketoconazole on cabozantinib plasma PK and effect of cabozantinib on CYP2C8 probe substrate rosiglitazone plasma PK. The Journal of Clinical Pharmacology 55(9): 1012-1023.

Oliveras-Ferraros C, Vazquez-Martin A, Colomer R, De Llorens R, Brunet J, and Menendez JA (2008) Sequence-dependent synergism and antagonism between paclitaxel and gemcitabine in breast cancer cells: the importance of scheduling. International journal of oncology 32(1): 113-120.

Ouerdani A, Struemper H, Suttle A, Ouellet D, and Ribba B (2015) Preclinical modeling of tumor growth and angiogenesis inhibition to describe pazopanib clinical effects in renal cell carcinoma. CPT: pharmacometrics & systems pharmacology 4(11): 660-668.

Pan F, Tian J, Zhang X, Zhang Y, and Pan Y (2011) Synergistic interaction between sunitinib and docetaxel is sequence dependent in human non-small lung cancer with EGFR TKIs-resistant mutation. Journal of cancer research and clinical oncology 137(9): 1397-1408.

Ricotti L, Tesei A, De Paola F, Ulivi P, Frassineti GL, Milandri C, Amadori D, and Zoli W (2003) In vitro schedule-dependent interaction between docetaxel and gemcitabine in human gastric cancer cell lines. Clinical cancer research : an official journal of the American Association for Cancer Research 9(2): 900-905.

Rocchetti M, Simeoni M, Pesenti E, De Nicolao G, and Poggesi I (2007) Predicting the active doses in humans from animal studies: a novel approach in oncology.

European journal of cancer 43(12): 1862-1868.

Signorelli M, Lissoni AA, De Ponti E, Grassi T, Ponti S, and Fruscio R (2015) Adjuvant sequential chemo and radiotherapy improves the oncological outcome in high risk endometrial cancer. Journal of gynecologic oncology 26(4): 284-292.

Simeoni M, De Nicolao G, Magni P, Rocchetti M, and Poggesi I (2013) Modeling of human tumor xenografts and dose rationale in oncology. Drug discovery today Technologies 10(3): e365-372.

Simeoni M, Magni P, Cammia C, De Nicolao G, Croci V, Pesenti E, Germani M, Poggesi I, and Rocchetti M (2004) Predictive pharmacokinetic-pharmacodynamic modeling of tumor growth kinetics in xenograft models after administration of anticancer agents. Cancer Res 64(3): 1094-1101.

Smith MR, De Bono JS, Sternberg CN, Le Moulec S, Oudard S, De Giorgi U, Krainer M, Bergman AM, Hoelzer W, and De Wit R (2015) Final analysis of COMET-1: Cabozantinib (Cabo) versus prednisone (Pred) in metastatic castration-resistant prostate cancer (mCRPC) patients (pts) previously treated with docetaxel (D) and abiraterone (A) and/or enzalutamide (E). Journal of Clinical Oncology 33: 7_suppl, 139.

Su Q, Li J, Ji X, Li J, Zhou T, Lu W, and Li L (2015) An LC-MS/MS method for the quantitation of cabozantinib in rat plasma: Application to a pharmacokinetic study. Journal of Chromatography B 985: 119-123.

Tai S, Sun Y, Squires JM, Zhang H, Oh WK, Liang CZ, and Huang J (2011) PC3 is a cell line characteristic of prostatic small cell carcinoma. The Prostate 71(15):

1668-1679.

Tamatani T, Ferdous T, Takamaru N, Hara K, Kinouchi M, Kuribayashi N, Ohe G, Uchida D, Nagai H, Fujisawa K, and Miyamoto Y (2012) Antitumor efficacy of sequential treatment with docetaxel and 5-fluorouracil against human oral cancer cells. International journal of oncology 41(3): 1148-1156.

Torre LA, Siegel RL, Ward EM, and Jemal A (2016) Global cancer incidence and mortality rates and trends—an update. Cancer Epidemiology and Prevention Biomarkers 25(1): 16-27.

Vaishampayan UN (2014) Development of cabozantinib for the treatment of prostate cancer. Core evidence 9: 61-67.

Vichai V, and Kirtikara K (2006) Sulforhodamine B colorimetric assay for cytotoxicity screening. Nature protocols 1(3): 1112-1116.

Wang D, Jiang Z, and Zhang L (2012) Concurrent and sequential administration of sunitinib malate and docetaxel in human non-small cell lung cancer cells and xenografts. Medical oncology (Northwood, London, England) 29(2): 600-606.

Wang Z, Zhao Z, Wu T, Song L, and Zhang Y (2015) Sorafenib-irinotecan sequential therapy augmented the anti-tumor efficacy of monotherapy in hepatocellular carcinoma cells HepG2. Neoplasma 62(2): 172-179.

Wu X, Gong S, Roy-Burman P, Lee P, and Culig Z (2013) Current mouse and cell models in prostate cancer research. Endocrine-related cancer 20(4): R155-170.

Yakes FM, Chen J, Tan J, Yamaguchi K, Shi Y, Yu P, Qian F, Chu F, Bentzien F, Cancilla B, Orf J, You A, Laird AD, Engst S, Lee L, Lesch J, Chou YC, and Joly AH

(2011) Cabozantinib (XL184), a novel MET and VEGFR2 inhibitor, simultaneously suppresses metastasis, angiogenesis, and tumor growth. Mol Cancer Ther 10(12): 2298-2308.

Yamazaki S, Nguyen L, Vekich S, Shen Z, Yin MJ, Mehta PP, Kung PP, and Vicini P (2011) Pharmacokinetic-pharmacodynamic modeling of biomarker response and tumor growth inhibition to an orally available heat shock protein 90 inhibitor in a human tumor xenograft mouse model. The Journal of pharmacology and experimental therapeutics 338(3): 964-973.

Footnotes

This work was supported by the National Natural Science Foundation of China. (Grant No. 81302831).

Figure Legends

Figure 1. In vitro cell inhibition effects of different treatment schedules on 22Rv1 and PC3 cells. A. Cell combination treatment schedules. PBS: phosphate buffer saline. B. Cell inhibition effects of different treatment schedules on 22Rv1 and PC3 cells.

Figure 2. Schematic of the integrated PK/PD model.

Figure 3. Plasma concentration-time profiles of docetaxel and cabozantinib in nude mice. A. Concentration-time profiles of Doc after a single dose (20mg/kg, i.v.) of Doc alone or Doc in combination with Cab (10mg/kg, p.o.) B. Concentration-time profiles of Cab after administering Cab at a dose of 10mg/kg/day by oral gavage alone or Cab in combination with Doc 20mg/kg/week, i.v. (mean ± SD, n=3)

Figure 4. Antitumor efficacy of different treated schedules on 22Rv1 tumor-bearing mice. Data were presented as the mean ± SD (n=5 or 6). A. Tumor volume changes over time. B. Tumor weight at the end of the treatment. C. Picture of excised tumors at the end of the treatment.

Figure 5. Antitumor efficacy of different treated schedules on PC3 tumor-bearing mice. Data were presented as the mean ± SD (n=5 or 6). A. Tumor volume changes over time. B. Tumor weight at the end of the treatment. C. Picture of excised tumors at the end of the treatment.

Figure 6. Visual predictive check (VPC) results of PK models. The black solid dots are the observed data. The black solid and dashed lines represent the medians of prediction and observed data, respectively. The dark grey dashed lines showed the 2.5th and 97.5th percentiles, and the light grey areas depicted the 95% predictive confidence intervals.

A. Single dose of 20 mg/kg Doc. B. Single dose of 20 mg/kg Doc in combination with 10 mg/kg Cab. C. Multiple dose of 10 mg/kg/day Cab.

Figure 7. Observed and model-simulated tumor volume-time profiles of 22Rv1 tumor-bearing mice stratified by group. The black solid dots are the observed data. The black solid lines represent the medians of prediction value, and the light grey areas depicted the 95% predictive confidence intervals. The black dashed lines showed the 2.5th, 50th and 97.5th percentiles respectively.

Figure 8. Observed and model-simulated tumor volume-time profiles of PC3 tumor-bearing mice stratified by group. The black solid dots are the observed data. The black solid lines represent the medians of prediction value, and the light grey areas depicted the 95% predictive confidence intervals. The black dashed lines showed the 2.5th, 50th and 97.5th percentiles respectively.

Figure 9. Combination index (φ) of each combination schedule obtained from PK/PD models (mean with 95% confidence interval).

Figure 10. Surface response plots relating Doc and Cab doses to tumor growth inhibition (% TGI) generated from simulation based on PK/PD models on day 28. A. Concurrent schedule “Doc + Cab” on 22Rv1 xenograft model. B. Sequential schedule “Doc ~ Cab” on 22Rv1 xenograft model. C. Concurrent schedule “Doc + Cab” on PC3 xenograft model. D. Sequential schedule “Doc ~ Cab” on PC3 xenograft model.

JPET Fast Forward. Published on October 30, 2017 as DOI: 10.1124/jpet.117.243931
This article has not been copyedited and formatted. The final version may differ from this version.

Table 1. Treatment schedules in vivo.

Group No.	Treatment group	Treatment description	Group category
22Rv1 xenograft mice			
(1)	Control	Control	Control
(2)	Doc 5	Doc 5 mg/kg/week	Monotherapy
(3)	Doc 10	Doc 10 mg/kg/week	Monotherapy
(4)	Cab 10	Cab 10 mg/kg/day	Monotherapy
(5)	Doc 5 + Cab 10	Doc 5 mg/kg/week and Cab 10 mg/kg/day, simultaneous administration	Concurrent schedule
(6)	Doc 10 + Cab 10	Doc 10 mg/kg/week and Cab 10 mg/kg/day, simultaneous administration	Concurrent schedule
(7)	Doc 5 6h Cab 10	Doc 5 mg/kg/week and Cab 10 mg/kg/day, with 6 hours interval	Interval schedule
(8)	Doc 10 6h Cab 10	Doc 10 mg/kg/week and Cab 10 mg/kg/day, with 6 hours interval	Interval schedule
(9)	Doc 10 ~ Cab 10	Doc 10 mg/kg/week for the first week, followed by Cab 10 mg/kg/day for the second week, and alternated weekly	Sequential schedule
PC3 xenograft mice			
(1)	Control	Control	Control
(2)	Doc 5	Doc 5 mg/kg/week	Monotherapy

(3)	Cab 10	Cab 10 mg/kg/day	Monotherapy
(4)	Doc 5 + Cab 10	Doc 5 mg/kg/week and Cab 10 mg/kg/day, simultaneous administration	Concurrent schedule
(5)	Doc 5 6h Cab 10	Doc 5 mg/kg/week and Cab 10 mg/kg/day, with 6 hours interval	Interval schedule
(6)	Doc 5 - Cab 10	Doc 5 mg/kg/week for the first week, followed by Cab 10 mg/kg/day for the second week, and alternated weekly	Sequential schedule
(7)	Cab 10 ~ Doc 5	Cab 10 mg/kg/day for the first week, followed by Doc 5 mg/kg/week for the second week, and alternated weekly	Sequential schedule

*All drug administration was conducted at 8:00 a.m. except the interval groups. For mice with concurrent schedule, Doc and Cab were administered simultaneously (8:00 a.m.) at the first day of every week. For mice with interval schedule, Cab was administered 6 hours after Doc injection (i.e. Doc was injected at 8:00 a.m. and Cab was given by gavage at 14:00 p.m.).

Table 2. Estimated PK parameters of docetaxel and cabozantinib

Parameters	**Definition**	**Estimate (RSE%)**	**IIV (CV%)**
Docetaxel			
CL (L/kg/h))	Clearance of central compartment	3.47 (11)	-
IC50_Cab (μg/L)	The concentration of Cab causing half of maximum impact on Doc CL	5270 (27)	-
Vc (L/kg)	Distribution volume of central compartment	0.977 (32)	-
Q (L/kg/h)	Clearance of distribution between central and peripheral compartment	3.21 (27)	-
Vp (L/kg)	Distribution volume of peripheral compartment	4.5 (15)	-
Residual error			
σ_1	Proportional error (CV%)	49.4 (10)	-
σ_2	Additive error (SD, μg/L)	-	-
Cabozantinib			
ka (h^{-1})	The absorption rate constant of cabozantinib	2.83 (22)	-
CL/F (L/kg/h))	Apparent clearance of cabozantinib	0.244 (9)	-
Vc/F (L/kg)	Apparent distribution volume of central compartment	1.37 (11)	-
Residual error			
σ_1	Proportional error (CV%)	34.8 (14)	-
σ_2	Additive error (SD, μg/L)	70.57 (25)	-

Table 3. PD parameters estimated from the 22Rv1 and PC3 xenografts PK/PD model.

Parameters	**Definition**	**22Rv1 Estimate (RSE%) (IIV, CV%)**	**PC3 Estimate (RSE%) (IIV, CV%)**
V0 (mm^3)	Initial tumor volume (control group) [a]	195 (7) (16.9)	145 (3) (2.7)
k_{ng} (h^{-1})	Tumor growth rate	0.0072 (6) (2.9)	0.0025 (9) (21.8)
KP (mm^3)	Tumor carrying capacity of 22Rv1 model	4560 (19) (4)	-
Nss (mm^3)	Tumor carrying capacity of PC3 model	-	2090 (16) (30)
k_{Doc} (h^{-1})	The anti-tumor effect coefficient of Doc	0.000206 (16) (38.9)	0.000289 (13) (30.3)
k1 (h^{-1})	Transit-rate constant (Doc monothetapy) [b]	0.0218 (34) (27)	0.0179 (16) (26.8)
$EC50_{Cab}$ (μg/L)	The concentration of Cab causing half of maximum inhibition on KP	399 (14) (31.9)	2210 (23) (62.1)
φ_1	Combination index of concurrent schedule	0.98 (11) (33.1)	1.25 (10) (21.8)
φ_2	Combination index of interval schedule	1.19 (11) (34.4)	1.34 (13) (30.8)
φ_3	Combination index of "Doc ~ Cab" sequential schedule	2.09 (18) (39.2)	3.63 (19) (42.4)
φ_4 [c]	Combination index of "Cab ~ Doc" sequential schedule	-	0.54 (21) (76.9)
σ_1 (CV% / SD)	Residual error of control group	9.2 / 15.9	- / 34.1
σ_2 (CV% / SD)	Residual error of Doc monotherapy	10.7 / -	5.5 / 6.9
σ_3 (CV% / SD)	Residual error of Cab monotherapy	7.2 / -	6.1 / 8.4
σ_4 (CV% / SD)	Residual error of concurrent schedule	9.4 / 16	3.1 / 10.8

JPET Fast Forward. Published on October 30, 2017 as DOI: 10.1124/jpet.117.243931
This article has not been copyedited and formatted. The final version may differ from this version.

σ_5 (CV% / SD)	Residual error of interval schedule	8.5 / 10.6	4.3 / 18.0
σ_6 (CV% / SD)	Residual error of "Doc ~ Cab"	10.9 / 6.4	- / 21.2
σ_7 (CV% / SD)	Residual error of "Cab ~ Doc "	-	5.6 / 18.3

[a] V0 estimated (RSE%) in 22Rv1 model were 212 (9), 230 (8), 178 (7), 196 (6) and 169 (13) for Doc, Cab, concurrent groups, interval groups and "Doc ~ Cab" sequential group respectively, and estimated in PC3 model were 122 (12), 112 (12), 97.8 (4), 105 (13), 132 (7) and 140 (15) for Doc, Cab, concurrent group, interval group, "Doc ~ Cab" and "Cab ~ Doc" sequential group, respectively.

[b] k1 estimated (RSE%) in 22Rv1 model were 0.0251 (7), 0.0306 (6) and 0.0183 (12) for concurrent groups, interval groups and "Doc ~ Cab" sequential group respectively, and estimated in PC3 model were 0.0061 (5), 0.0272 (10), 0 and 0.0271 (21) for concurrent group, interval group, "Doc ~ Cab" and "Cab ~ Doc" sequential group, respectively.

[c] A subject was removed during the modeling process since its φ approximated to 0.

JPET Fast Forward. Published on October 30, 2017 as DOI: 10.1124/jpet.117.243931
This article has not been copyedited and formatted. The final version may differ from this version.

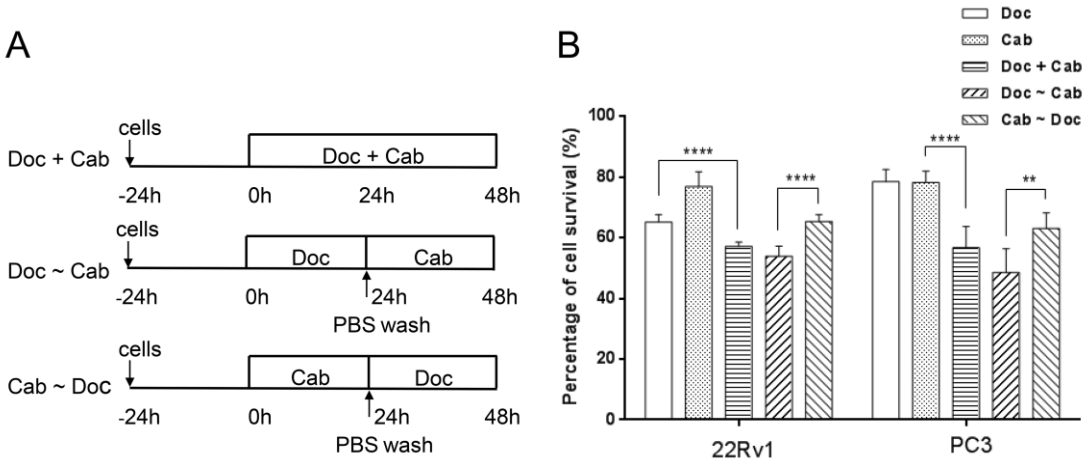

Figure 1

JPET Fast Forward. Published on October 30, 2017 as DOI: 10.1124/jpet.117.243931
This article has not been copyedited and formatted. The final version may differ from this version.

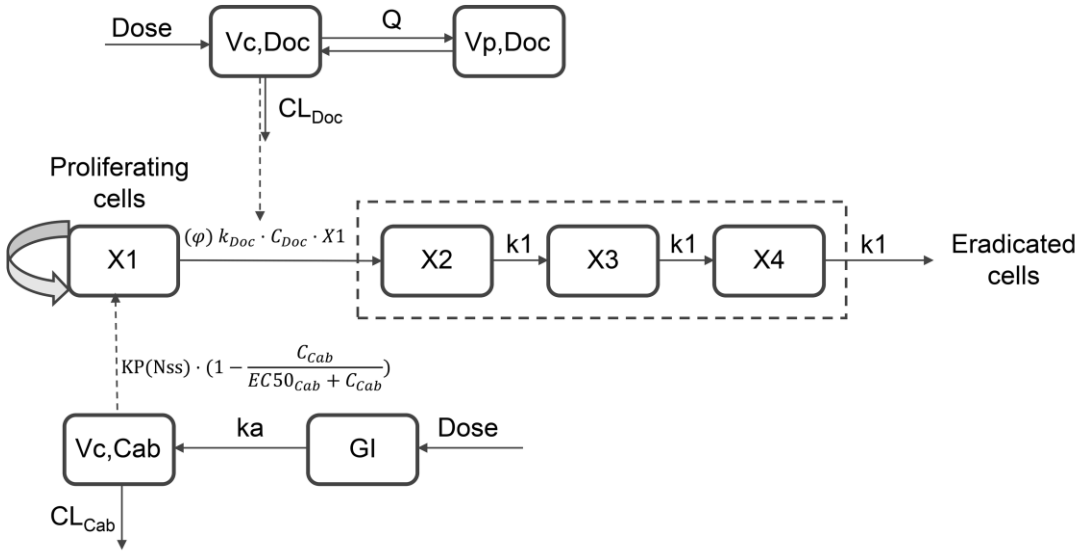

Figure 2

JPET Fast Forward. Published on October 30, 2017 as DOI: 10.1124/jpet.117.243931
This article has not been copyedited and formatted. The final version may differ from this version.

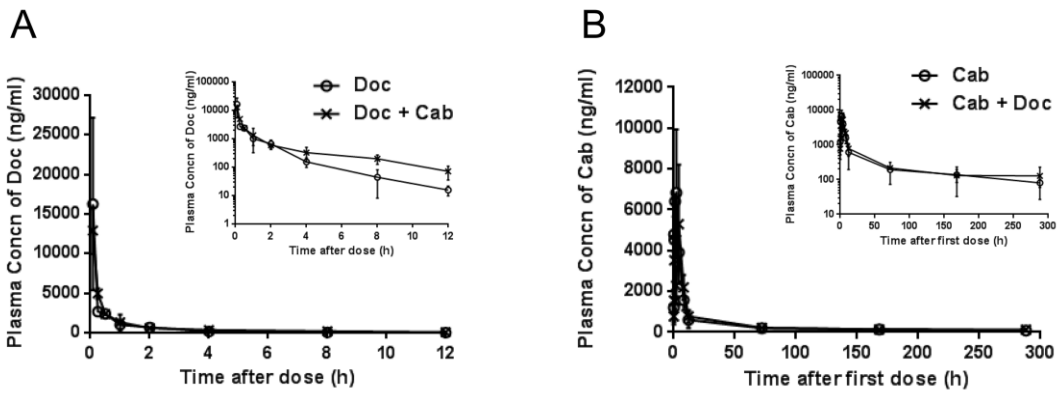

Figure 3

JPET Fast Forward. Published on October 30, 2017 as DOI: 10.1124/jpet.117.243931
This article has not been copyedited and formatted. The final version may differ from this version.

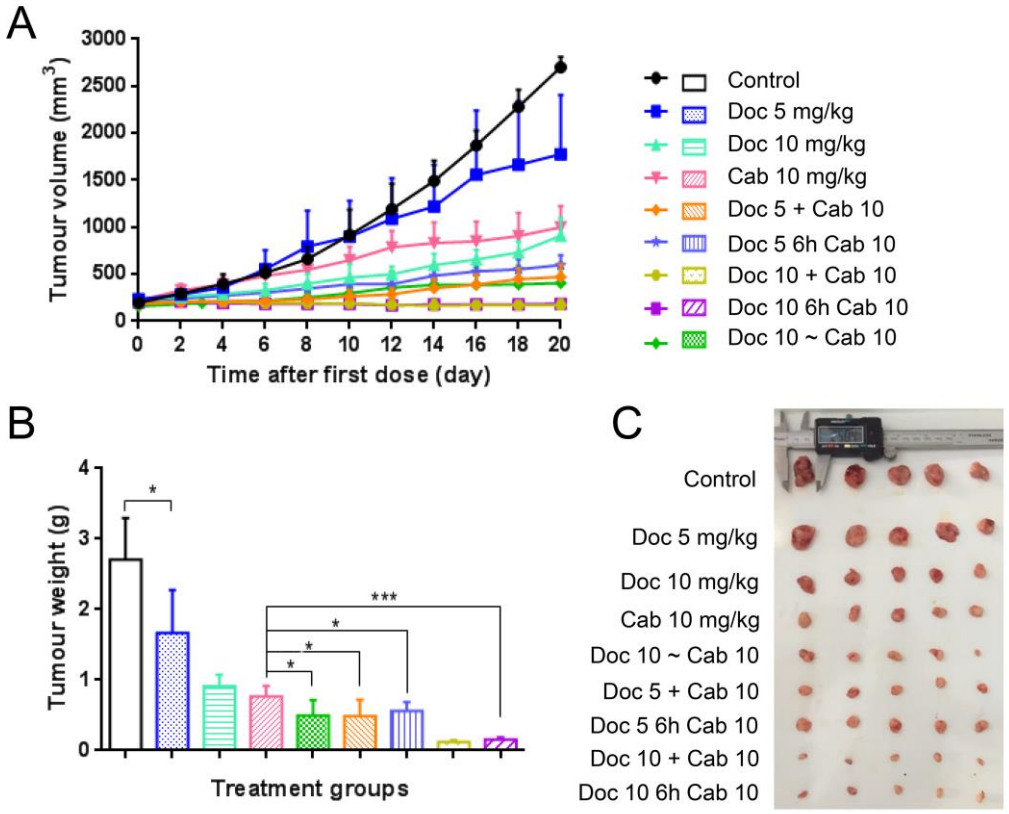

Figure 4

JPET Fast Forward. Published on October 30, 2017 as DOI: 10.1124/jpet.117.243931
This article has not been copyedited and formatted. The final version may differ from this version.

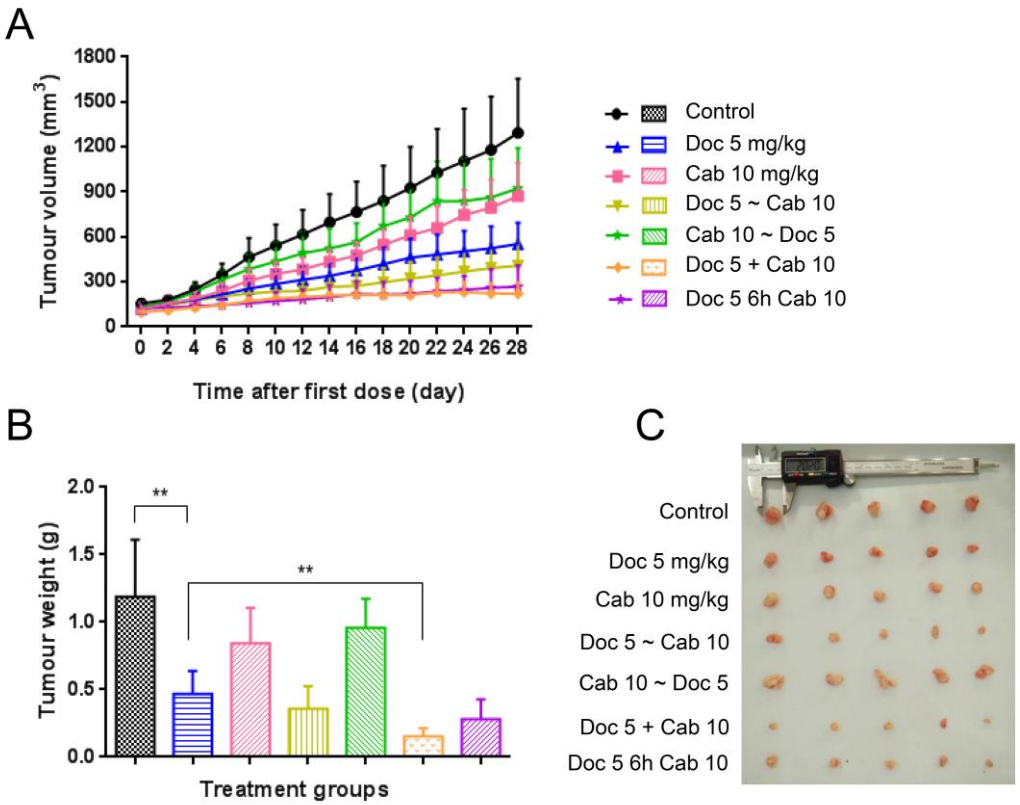

Figure 5

JPET Fast Forward. Published on October 30, 2017 as DOI: 10.1124/jpet.117.243931
This article has not been copyedited and formatted. The final version may differ from this version.

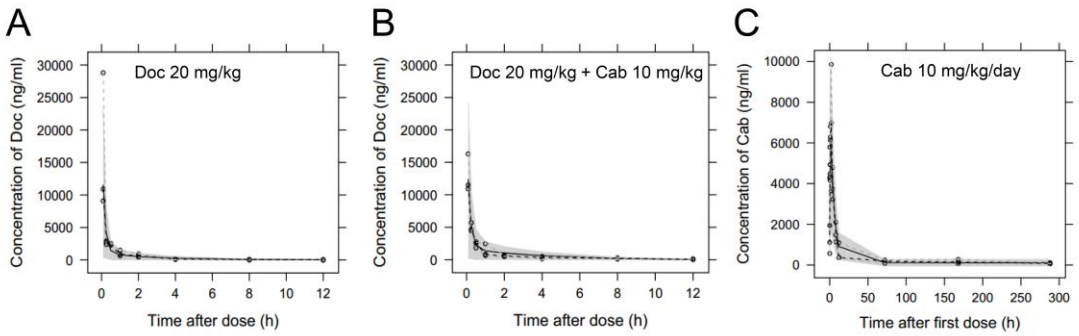

Figure 6

JPET Fast Forward. Published on October 30, 2017 as DOI: 10.1124/jpet.117.243931
This article has not been copyedited and formatted. The final version may differ from this version.

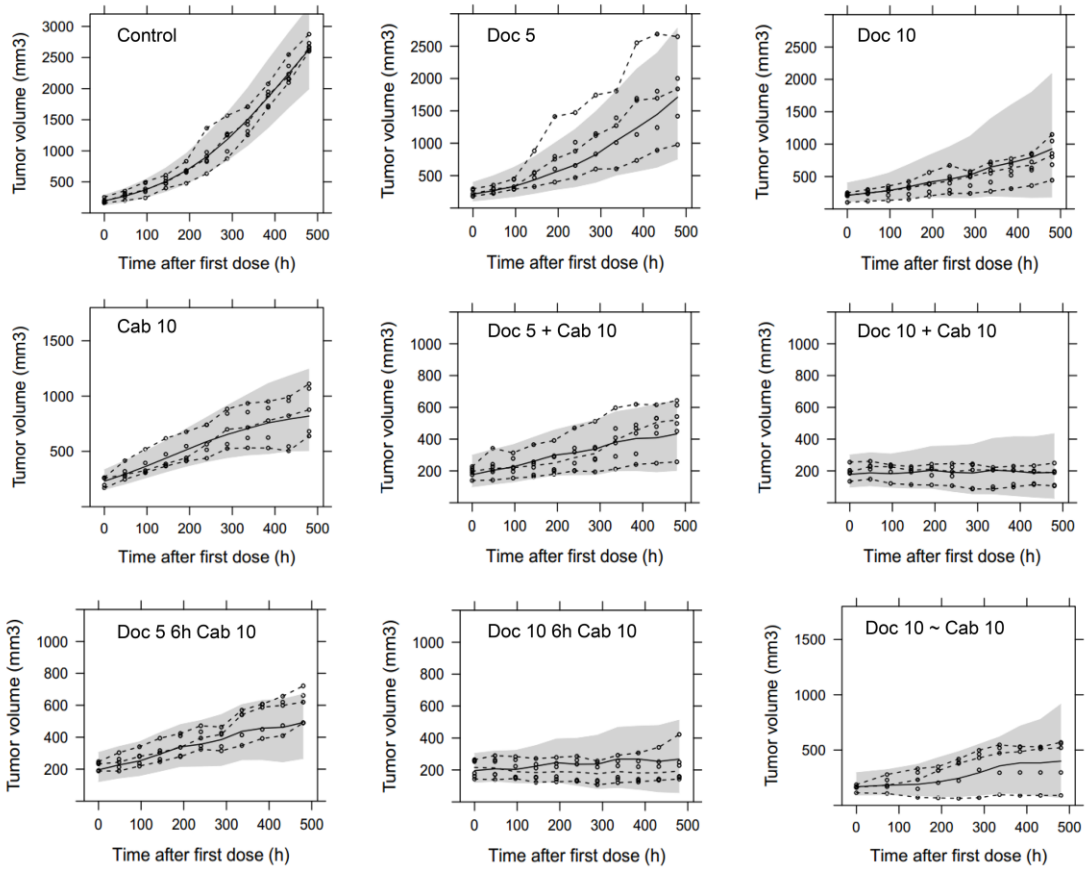

Figure 7

JPET Fast Forward. Published on October 30, 2017 as DOI: 10.1124/jpet.117.243931
This article has not been copyedited and formatted. The final version may differ from this version.

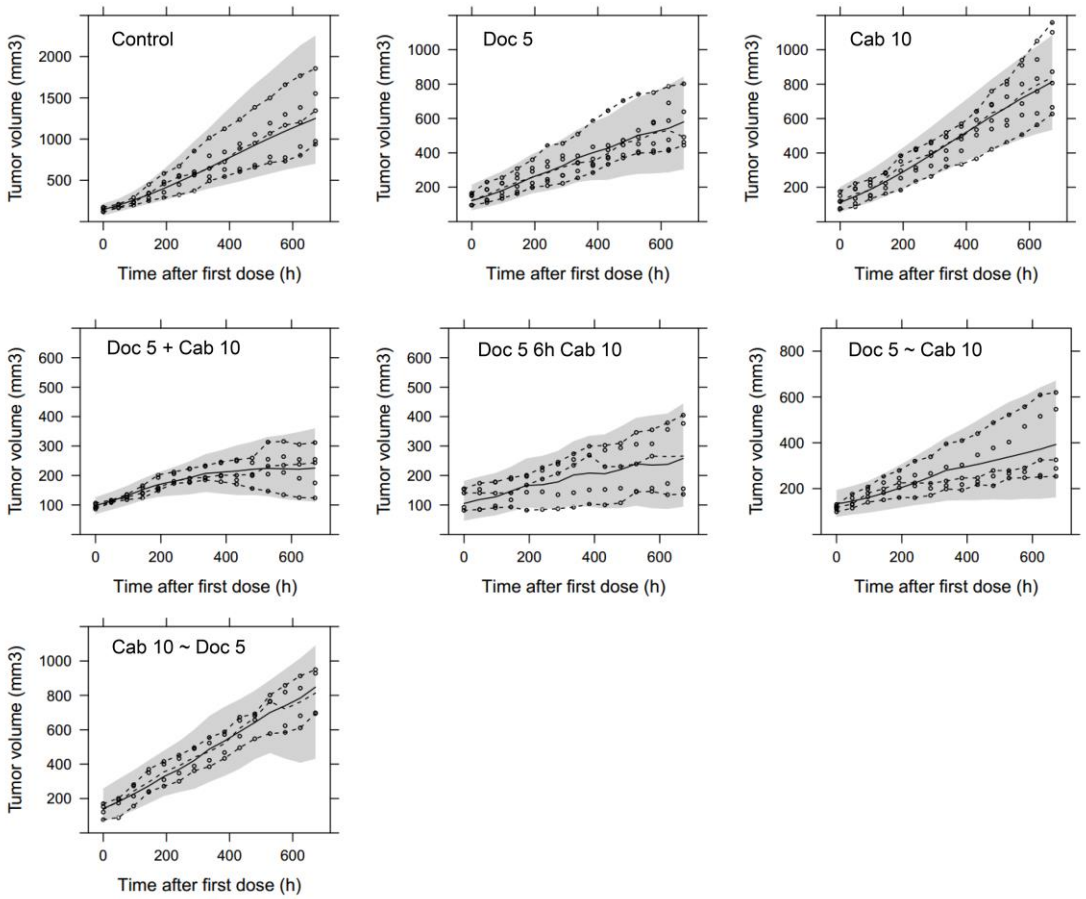

Figure 8

JPET Fast Forward. Published on October 30, 2017 as DOI: 10.1124/jpet.117.243931
This article has not been copyedited and formatted. The final version may differ from this version.

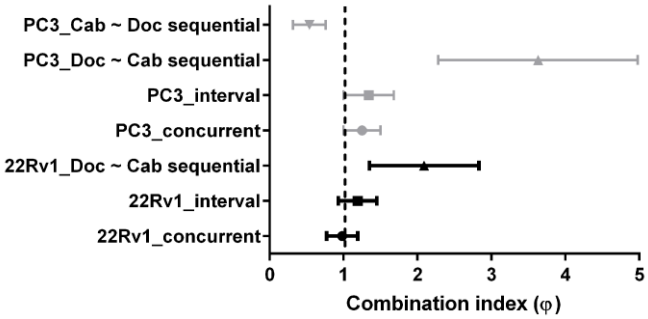

Figure 9

JPET Fast Forward. Published on October 30, 2017 as DOI: 10.1124/jpet.117.243931
This article has not been copyedited and formatted. The final version may differ from this version.

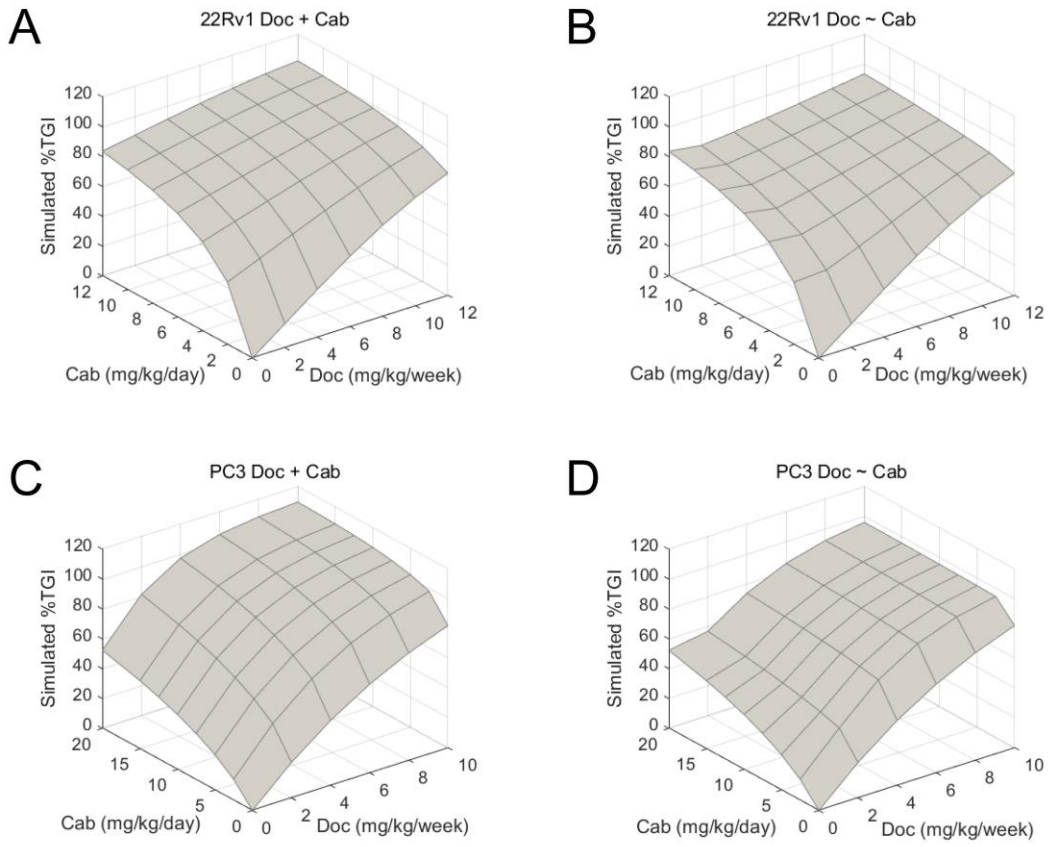

Figure 10

Supplementary Tables and Figures of manuscript "Pharmacokinetic/ Pharmacodynamic Modeling of Schedule-Dependent Interaction between Docetaxel and Cabozantinib in Human Prostate Cancer Xenograft Models"

Table S1. PD parameters obtained from the 22Rv1 xenografts PK/PD model with or without PK interaction.

Parameters	**Definition**	**Without PK interaction Estimate (RSE%)**	**With PK interaction Estimate (RSE%)**
V0 (mm^3)	Initial tumor volume	195 (7)	195 (7)
k_{ng} (h^{-1})	Tumor growth rate	0.0072 (6)	0.0072 (6)
KP (mm3)	Tumor carrying capacity	4560 (19)	4560 (19)
k_{Doc} (h^{-1})	The anti-tumor effect coefficient of Doc	0.00018 (20)	0.000206 (18)
k1 (h^{-1})	Transit-rate constant	0.0217 (9)	0.0218 (34)
$EC50_{Cab}$ (ug/L)	The concentration of Cab causing half of maximum inhibition on KP	399 (14)	399 (14)
φ_1	Combination index of concurrent schedule	1.57 (10)	0.978 (11)
φ_2	Combination index of interval schedule	1.3 (11)	1.19 (11)
φ_3	Combination index of "Doc 10 ~ Cab 10" sequential schedule	2.1 (17)	2.09 (18)

Table S2. PD parameters obtained from the PC3 xenografts PK/PD model with or without PK interaction.

Parameters	**Definition**	**Without PK interaction** **Estimate (RSE%)**	**With PK interaction** **Estimate (RSE%)**
V0_C (mm^3)	Initial tumor volume of control group	145 (3)	145 (3)
k_{ng} (h^{-1})	Tumor growth rate	0.0025 (9)	0.0025 (9)
Nss(mm3)	Tumor carrying capacity	2090 (16)	2090 (16)
k_{Doc} (h^{-1})	The anti-tumor effect coefficient of Doc	0.000254 (12)	0.000289 (13)
k1 (h^{-1})	Transit-rate constant	0.0178 (17)[a]	0.0179 (16)
$EC50_{Cab}$ (ug/L)	The concentration of Cab causing half of maximum inhibition on KP	2210 (23)	2210 (23)
φ_1	Combination index of "Doc 5 + Cab 10" concurrent schedule	2 (10)	1.25 (10)
φ_2	Combination index of "Doc 5 6h Cab 10" interval schedule	1.46 (14)	1.34 (13)
φ_3	Combination index of "Doc 5 ~ Cab 10" sequential schedule	3.61 (19)	3.63 (19)
φ_4	Combination index of "Cab 10 ~ Doc 5" sequential schedule	0.535 (40)	0.537 (21)

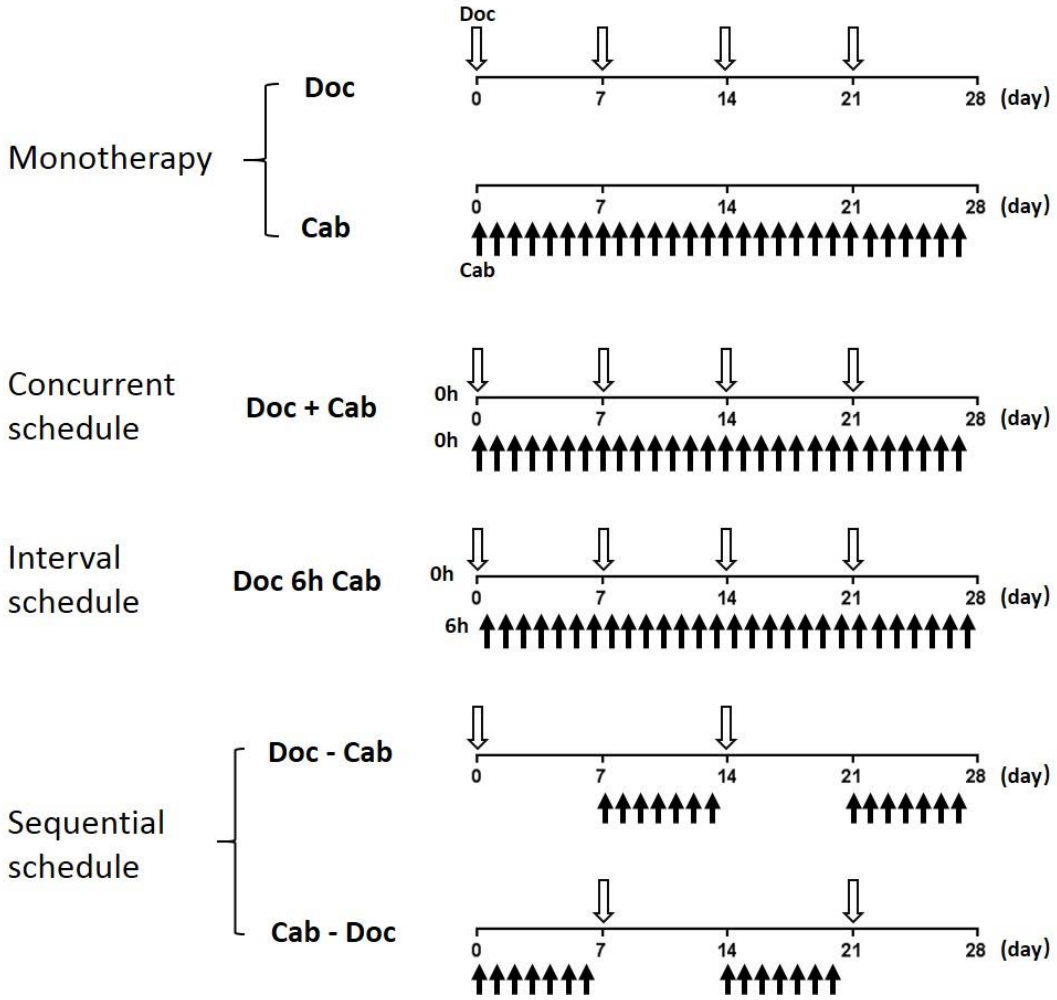

Figure S1. Schematic diagram of treatment schedules in vivo. Hollow arrows represent docetaxel injection, and black solid arrows represent cabozantinib administration.

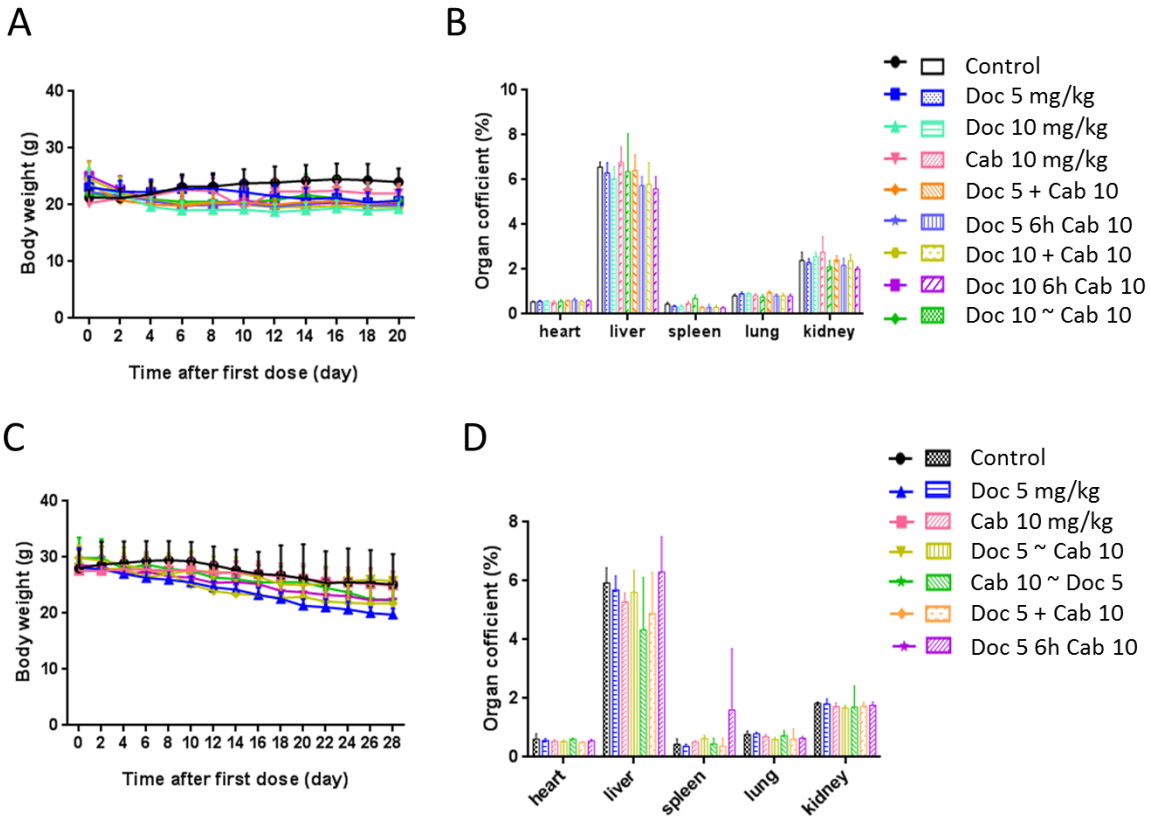

Figure S2. Safety evaluation of different treatment schedules on 22Rv1 and PC3 tumor-bearing mice. A. Body weight of 22Rv1 tumor-bearing mice during treatment. B. Organ coefficient of 22Rv1 tumor-bearing mice on day 21. C. Body weight of PC3 tumor-bearing mice during treatment. D. Organ coefficient of PC3 tumor-bearing mice on day 28.

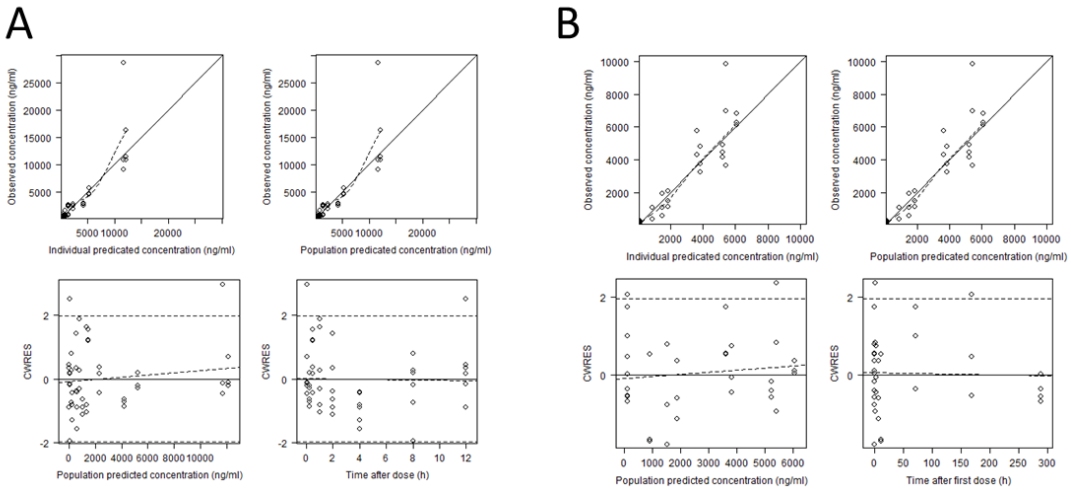

Figure S3. Goodness-of-fit (GOF) plots of PK model. A. GOF plots of docetaxel PK model. B. GOF plots of cabozantinib PK model.